

# Experimental analysis on the risk of vortex ventilation and the free surface ventilation of marine propellers

Anna Maria Kozłowska<sup>1,3</sup>, Sverre Steen<sup>2,3</sup>

<sup>1</sup>Department of Marine Technology, NTNU, 7491 Trondheim, Trondheim, Norway, [anna.kozłowska@ntnu.no](mailto:anna.kozłowska@ntnu.no)

<sup>2</sup>Department of Marine Technology, NTNU, 7491 Trondheim, Trondheim, Norway, [sverre.steen@ntnu.no](mailto:sverre.steen@ntnu.no)

<sup>3</sup>Rolls Royce University Technology Centre “Performance in a Seaway”, Trondheim, Norway

## ABSTRACT

The paper presents a discussion of the ventilation inception and air drawing prediction of ships propellers, aiming to predict under what conditions ventilation will happen, and the actual physical mechanism of the ventilation.

Three different types of ventilation inception mechanisms are included in our discussion: free surface vortex ventilation, ventilation by sucking down the free surface without forming a vortex as well as ventilation by propeller coming out of the water. Ventilation prediction is based on a series of model tests, where the propeller is tested in different levels of intermittent ventilation. The use of underwater video gives a visual understanding of the ventilation phenomena.

Ventilation by vortex formation has analogies with other phenomena, such as the inlet vortex in pump sumps, ground vortex at the inlet of the aircraft engines and the Propeller Hull Vortex Cavitation (PHVC). The paper includes comparison between Propeller Hull Vortex Cavitation (PHVC) and Propeller Free Surface Vortex Ventilation (PFSVV) as well as comparison between PFSVV and vortex formations of aero engines during high power operation near a solid surface. Experimental data based on several different model tests shows the boundary between the vortex forming, non-vortex forming and free surface ventilation flow regimes. For comparison the following parameters, which determined the intensity of the hydrodynamic interaction between the propeller and free surface have been used: propeller load coefficient  $c_T$ , tip clearance ratio  $c/D$ , propeller submergence ratio  $h/R$ , ambient velocity  $V_i$  and flow cavitation/ventilation number  $\sigma_{cav} / \sigma_{vent}$ .

## Keywords

Vortex ventilation, propeller hull vortex cavitation, boundaries, empirical relations, ventilation inception, model tests

## SYMBOLS INDEX

$a_v$	[m]	vortex radius	P/D	[-]	propeller pitch ratio
$c$	[m]	tip clearance, distance from the top of propeller disk to the surface (hull)	PFSVV	[-]	propeller free surface vortex ventilation
$c/D$	[-]	tip clearance ratio	PHVC	[-]	Propeller hull vortex cavitation
$c_T$	[-]	propeller load coefficient	$\Gamma$	[m <sup>2</sup> /s]	span-wise circulation
$c_{Tn}$	[-]	propeller load coefficient for non-ventilated deeply submerged propeller	$p_v$	[Pa]	vapor pressure
$c_{0.7}$	[m]	chord length at 0.7R	$p_o$	[Pa]	atmospheric pressure
$c_{L0.7}$	[m]	lift coefficient at 0.7R	S	[N/m]	Surface tension of the water
$D, R$	[m]	propeller diameter, propeller radius	$T$	[N]	propeller thrust
$h$	[m]	propeller submergence from the propeller axis to the free surface	$V_A$	[m/s]	speed of advance
$h/R$	[-]	propeller submergence from the propeller axis to the free surface	$V_i$	[m/s]	velocity through the propeller disk
$J$	[-]	advance number	$V_0$	[m/s]	free stream velocity
$J_c$	[-]	critical advance coefficient	$z$	[-]	number of blades
$J_{sc}$	[-]	super critical advance coefficient	$\beta_T$	[-]	total thrust loss factor
$K_T$	[-]	thrust coefficient	$\sigma_{cav}$	[-]	cavitation number
$K_{Tn}$	[-]	time-averaged mean value of the thrust coefficient for deeply submerged non-ventilated propeller.	$\sigma_{vent}$	[-]	ventilation number
$n$	[Hz]	propeller revolutions	$\rho$	[kg/m <sup>3</sup> ]	density of water
			$\nu$	[m <sup>2</sup> /s]	kinematic viscosity

$J = V_A/n \cdot D$  – advance coefficient

$K_T = \frac{T}{\rho n^2 D^4}$  – thrust coefficient

$c_T = \frac{8}{\pi} \cdot \frac{K_T}{J^2}$  – propeller load coefficient

$c = (h - R)$  – tip clearance, distance from the top of propeller disk to the free surface (hull)

$\sigma_{cav} = \frac{p_o - p_v}{0.5\rho(V_A)^2}$  – cavitation number (propeller axis is the reference pressure for the cavitation number)

$\sigma_{vent} = 2gh/(V_\infty)^2$  – ventilation number

$We = nD\sqrt{\rho D/S}$  – Weber number

## 1. INTRODUCTION

When a ship propeller operates under highly loaded condition, unsteady line vortex cavitation may occur between the propeller tip and the hull. This type of cavitation is known as propeller - hull vortex cavitation (PHVC) and, if it occurs, it causes strong vibrations and noise in the stern of the ship. When a propeller is operating close to the free water surface, a vortex might form between the propeller and the free surface through which air can be drawn down to the propeller, so that it ventilates – a phenomenon we call Propeller Free Surface Vortex Ventilation (PFSVV). Ventilation typically occurs when the propeller loading is high and the propeller submergence is limited, and when the relative motions at the propeller are large due to heavy seas. Propeller ventilation inception depends on different parameters i.e. propeller loading, forward speed and the distance from the propeller to the free surface, see for instance Califano (2011), Smogeli (2006), Koushan (2006), Kozłowska et.al. (2009) and Kozłowska and Steen (2010). It is likely that the physical phenomena causing vortex forming of PHVC and vortex ventilation are closely related, see Huse [5]. In this paper, PFSVV will be compared to PHVC with the aim of getting a better understanding of the physical mechanisms causing PFSVV, and on that basis enable the making of better simulation and prediction methods for PFSVV.

Ventilation by vortex formation (PFSVV) has been studied by several researchers see for instance Koushan (2006 I, II and III), Kozłowska et.al. (2009), Kozłowska and Steen (2010), Califano (2011), Koushan et.al. (2011) and Kozłowska et.al. (2011). Koushan (2006) performed extensive model tests on an azimuth thruster with 6 DoF measurements of forces on one of the four blades on an azimuthing thruster, as reported in three papers (Koushan 2006 I, II and III). Koushan (2006 I) described the dynamics of ventilated propeller blade axial force on pulling thruster at bollard condition running at several constant immersion ratios and constant propeller rate of revolution. Koushan (2006 II) presented the dynamics of ventilated propeller blade axial force on a pulling thruster at bollard condition and constant propeller rate of revolution in forced sinusoidal heave motion. Koushan (2006 III) presented the dynamics of ventilated propeller blade and duct loadings at bollard condition and constant propeller rate of revolution.

Kozłowska et.al. (2009) focused on ventilation inception mechanisms, classification of different types of ventilation, thrust loss related to each type of ventilation, and provided a simple calculation method for predicting thrust loss.

Kozłowska and Steen (2010) focused on comparison between ventilation in static and dynamic conditions (heave motion) both for open and ducted propeller, and discussed how to estimate thrust loss. As a conclusion, a new formulation of the relations between ventilation and thrust loss was developed.

Kozłowska et.al. (2011) presented comparison between model tests and numerical calculations of thrust loss due to ventilation. The comparison contains two main aspects: comparison between blade forces and moments during non-ventilating and ventilating phase and comparison of results of flow visualization using high speed video (experiments) with CFD simulation results. The comparisons aim at identifying the degree of correlation and discuss reasons for deviations.

PFSVV occurs for completely submerged, highly loaded propellers at low advance speed. The vortex funnel can reach the surface quite far from the propeller disc, especially for large submergence ratios. *Figure 1* shows two examples of PFSVV. Note that submergence  $h$  is the distance from the undisturbed free surface to the propeller axis.

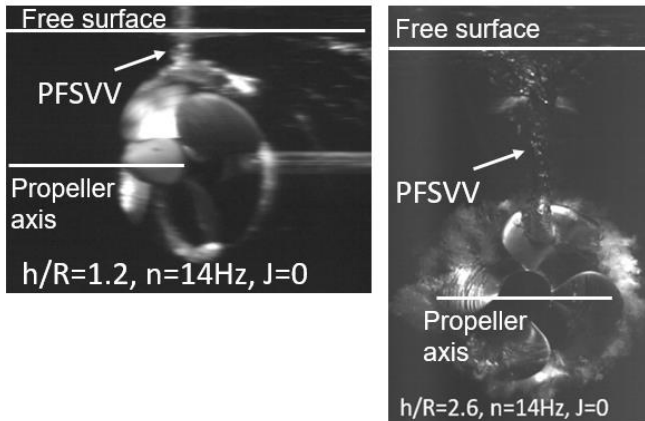


Figure 1: Impact of the free surface ventilation (PFSVV) for complete submerged propellers

The PHVC phenomenon was first reported by Huse [5]. Systematic observations had been carried out to investigate the effect of the afterbody form, tip clearance  $c/D$ , propeller loading  $c_T$  and cavitation number  $\sigma_{cav}$ . Experimental observation with a flat, horizontal plate above the propeller in a cavitation tunnel showed that PHVC is more likely to occur for small tip clearances (up to 20% of propeller diameter,  $c=0.2D$ ) for low advance coefficient  $J$ .

Based on experimental investigations four hypotheses have been suggested for criteria leading to PHVC: a so called “starting vortex”, “vortices created by the shear flow in the wake field”, “vortices created in other regions of the flow field” as well as “the pirouette effect”, see Figure 2. The “Starting vortex” hypothesis is based on Helmholtz’s second theorem, which states that a vortex must be either closed or terminate on the boundary of the fluid. Figure 2 below shows the corresponding vortex line representation of a propeller blade. Circulation will also be closed on the shortest possible way. This means that the tip clearance must be less than the blade length and axial flow velocity in the region between hull and blade tip should be close to zero. Hypothesis based on “vortices created by shear flow in the wake field” means that a high wake peak in the upper part of the propeller disk gives rise to intense shear flow in the region of highest velocity gradient. This represents a vorticity in the flow field that may “curl up” to form the concentrated vortices necessary to create PHVC.

The basic idea for the hypothesis based on “vortices created in other regions of the flow field” is that the cores of vortices will cavitate when entering the low pressure region between propeller and hull.

Huse [5] concluded that the hypothesis based of the “pirouette effect” is probably the most correct. By this hypothesis the effect of tip clearance, randomness, effect of blade angular position and effect of vertical fins can be satisfactory explained. The basic phenomena related to “pirouette effect” were further explain later by Martio et.al. [12]. As the gap between the propeller blade tip and the wall is decreased, the blade suction side does not obtain enough water from the inlet side, so water is also sucked from downstream, causing a rotation of the flow, which is concentrated into a vortex by the so-called pirouette effect (rotational velocity has to increase considerably in order to keep the angular momentum constant, when the radius is reduced, thus forming a marked vortex) and finally causing the PHVC inception.

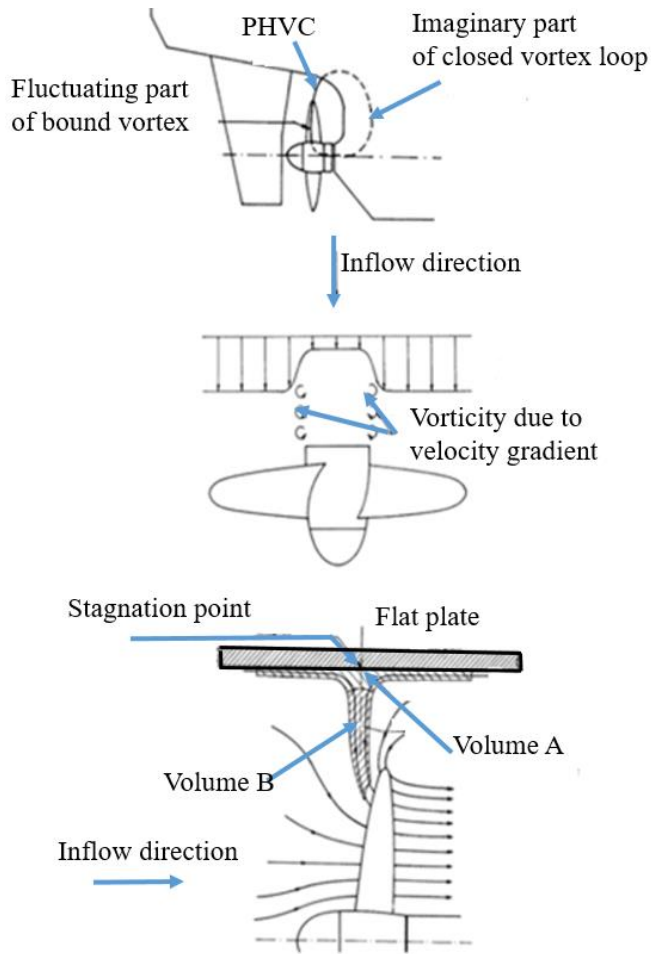


Figure 2: “starting vortex” (top), “vortices created by the shear flow in the wake field (middle) and “pirouette effect (bottom) hypothesis illustration, Huse [5]

A more systematic investigation of the PHVC phenomena has been carried out by Sato et. al. [17] and Nishiyama [14]. Sato et. al. [17] presented observation of flow on horizontal flat plate above a working propeller to understand propeller hull vortex cavitation. Air bubbles were injected into the flow field in order to visualize streamlines of the plate. As a continuation of his work the flow patterns were simulated by a RANS methods by Martio et.al. [12]. The agreement between the observations and computational results was considered to be satisfactory.

Another phenomenon with similarities to PFSVV is the occurrence of ground vortices for aero engines, and it is of interest to see if the knowledge on ground vortices can be applied to PFSVV. The threshold of formation of so-called ground vortices for aero engines during high power operation near a solid surface has been investigated since 1985 i.e., see for instance Nakayama and Jones [13] and Jermy and Ho [7]. The factors determining the formation of vortex include engine thrust, distance from the ground and the ambient velocity are presented in Figure 3. The threshold of vortex formation numerically predicted agrees with previous wind tunnel studies

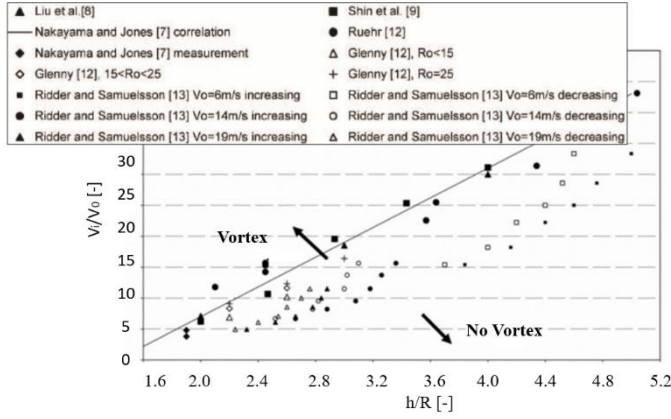


Figure 3: Experimental data showing the boundary between the vortex forming and non-vortex forming flow regimes, *Jermy and Ho* [7] as the function of the distance from the inlet center to the ground divided by inlet radius ( $h/R$ ) and the inlet velocity divided by ambient velocity ( $V_i/V_o$ ).

This paper focuses on the boundary between vortex forming, non - vortex forming, and the free surface ventilation of marine propellers. Results of four different experimental campaigns are applied in this paper. The naming convention given in *Table 1* is used.

Author	Year	Acronym	Publications
Kozłowska & Califano	2009	<i>Koz09</i>	<i>Califano [2]</i>
Kozłowska	2010	<i>Koz10</i>	<i>Kozłowska et.al. [11]</i>
Kourosh & Spence	2010	<i>Kou10</i>	<i>Koushan et.al. [8]</i>
Kozłowska	2016	<i>Koz16</i>	<i>Presented in this paper</i>

Table 1: Test campaigns

The majority of the results presented were obtained during the test campaign *Koz16*. Some cases from the other three test campaigns were used for comparison or to investigate missing cases relevant to this study. The *Koz16* test campaign is described in *Chapter 2* below.

Test campaign (*Koz09*), previously published by Califano [2], were conducted at submergence ratios  $1.0 \leq h/R \leq 2.9$  in the Marine Cybernetics Laboratory at the Marine Technology Centre, having dimensions (length  $\times$  breadth  $\times$  depth) of 40m $\times$ 6.45m $\times$ 1.5m. The carriage speed  $U$  and the propeller shaft frequency  $n$  were varied in order to obtain advance ratios  $J$  around 0.1. The propeller (P1374) had a diameter of 250mm, blade area ratio equal to 0.6 design pitch ratio  $P/D=1.1$ , the propeller hub diameter was 65mm. During measurements images were acquired with a high speed camera at sampling frequencies in the range between 60 and 480 Hz, depending on the test conditions. The test campaign (*Koz10*), published by Kozłowska et.al. [11] were conducted in the large towing tank at the Marine Technology Centre, having dimensions (length  $\times$  breadth  $\times$  depth) of 260m $\times$ 10.5m $\times$ 5.6m. Tests were conducted for four submergence ratios  $h/R=2.5, 1.5, 1.0, 0$ . For all four submergences the carriage speed was varied in order to obtain the following advance ratios  $J=0, 0.15, 0.3, 0.45, 0.6, 0.75, 0.9, 1.05, 1.2$ . Propeller revolution speed was constant and equal to 18 Hz. The propeller (P1440) had a diameter of 200 mm, design pitch ratio of 1.2 and expanded area ratio of 0.447. The test campaign (*Kou10*) was published by Koushan et.al. [8]. The same propeller model as for test campaign (*Koz10*) was used for experiments. Test were conducted in the large towing tank at the Marine Technology Centre in calm water and two different propeller submergences  $h/R=2.5$  and  $h/R=1.0$ . Propeller revolution speed was constant and equal to 18 Hz. For all four submergences, the carriage speed was varied in order to obtain the advance ratios in the range  $0 \leq J \leq 1.2$ .

## 2. TEST SET UP AND INSTRUMENTATION

The *Koz16* test was performed in the large towing tank at the Marine Technology Centre. A four-bladed, right handed propeller model (P1374) was used. The propeller has a diameter of 250 mm, blade area ratio equal to 0.6 design pitch ratio  $P/D=1.1$  and the propeller hub diameter is 65mm.

A conventional Kempf and Remmers two-components propeller open water dynamometer was used to measure propeller thrust and torque. Due to the torque (15Nm) and force (400N) limits of the dynamometer the range of  $J$  values for the higher revolutions speeds had to be limited, the limits are given in *Table 2* below.

$n[rps]$	9 rps	12 rps	14 rps	16 rps
Max Thrust: $T[N]$	194N	345 N	368N	335N
Max Torque: $Q[Nm]$	7.1Nm	12.7Nm	14.2Nm	14.3Nm
$J[-]$	0	0	0.3	0.6

*Table 2: Lower limits of advance number  $J$  due to the torque and thrust limits of the dynamometer. The max thrust and torque values are the maximum values measured during the experiments.*

During measurements, images are acquired with two high speed cameras (top and suction side view of the propeller) at a sampling frequency of 200 Hz. The cameras were controlled by a dedicated computer providing trigger pulses in order to extract time stamps for the acquired images. *Figure 4* shows a picture of the test set-up and a sample of the pictures from above-and underwater videos.

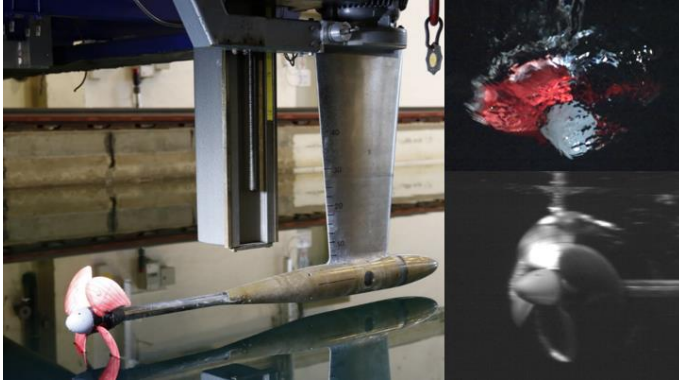


*Figure 4: Test set up (left) and propeller view from underwater (bottom right) and above water camera (top right)*

The necessary light for the camera acquisition system is provided by two lamps: one above the water surface and one underwater. The signals were acquired at a sampling frequency of 200 Hz using a 20 Hz low-pass Butterworth filter. Tests were performed at different draughts and propeller speeds. The draught is defined as submergence of the propeller center  $h$  divided by propeller radius  $R$ . For each draught and propeller speed the propeller was tested at different advance numbers, ranging from the lower limit specified in *Table 2* to  $J = 1.0$ . The different advance numbers were obtained at various propeller speeds so that for the same advance numbers different propeller thrust were obtained, thus varying the Weber number. Weber number ( $We$ ) is square root ratio of the inertia force to the force of surface tension and is defined as  $We = nD\sqrt{\rho D/S}$ , where  $n$  is number of propeller revolutions,  $D$  is propeller diameter,  $\rho$  is density of the water and  $S$  is surface tension of the water. According to Shiba (1953) the influence of Weber's number disappears above the so-called minimum Weber's number, which is about 180. Full scale propellers operate well above Weber's number 180 but for model scale tests Weber's number could be lower than minimum values. In our case only for propeller revolution speeds over  $n=13Hz$ , the influence of Weber's number can be neglected, when following the advice by Shiba (1953). The complete test matrix is given in *Table 3* below.

$n$ [rps]	9 rps	12 rps	14 rps	16 rps
$J$ [-]	0 – 1.0	0 – 1.0	0.3 – 1.0 for $h/R > 1.4$ 0 – 1.0 for $h/R \leq 1.4$	0.6 – 1.0 for $h/R > 1.2$ 0 – 1.0 for $h/R \leq 1.2$
$V_A$ [-]	0 – 2.25	0 – 3.0	1.05 – 3.5 for $h/R > 1.4$ 0 – 3.5 for $h/R \leq 1.4$	2.4 – 4.0 for $h/R > 1.2$ 0 – 4.0 for $h/R \leq 1.2$
$h/R$ [-]	-0.5, 0, 0.5, 1.0, 1.2, 1.4, 1.5, 1.6, 1.8	-0.5, 0, 0.5, 1.0, 1.2, 1.4, 1.5, 1.6, 2.0	-0.5, 0, 0.5, 1.0, 1.2, 1.4, 1.5, 1.6, 2.0	-0.5, 0, 0.5, 1.0, 1.2, 1.4, 1.5, 1.6, 2.0

Table 3: Test Matrix

### 3. COMPARISON BETWEEN GROUND VORTEX INLET FORMATION AND PROPELLER VENTILATION

#### 3.1 Propeller ventilation

Propeller ventilation by vortex formation has analogies to the inlet vortex. Using the same parameters for propeller and suction inlet, see *Figure 3*, the borderline between the vortex forming, non-vortex forming and free surface ventilation flow regimes for marine propellers can be drawn.

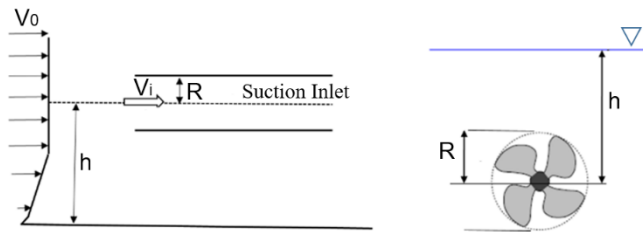


Figure 5: A sketch showing principal parameters,  $(V_i/V_o)$  and  $(h/R)$

Following the work for inlet vortices, the experimental results for model propellers are compared in order to compare the criteria between vortex forming, non - vortex forming and free surface ventilation flow regimes of marine propellers.

Two factors, which determined the formation of the vortex, were investigated as for the inlet vortex: propeller radius divided by the distance from the propeller centre to the free surface  $h/R$  and the velocity through the propeller disk  $V_i$  divided by the free stream velocity  $V_o$ ,  $V_i = V_o + 0.5(-V_o + \sqrt{V_o^2 + \frac{2T}{\rho_4^2 D^2}})$ , see *Figure 5*.

Experimental data based on the different model tests listed in *Table 1* show the boundary between the vortex forming, non-vortex forming and free surface ventilation flow regimes. The type of ventilation is identified visually, either directly or from the video recordings. The effect of the vortex formation for marine propellers during transient operation near free surface is presented in *Figure 6* below. The factors determining the formation of a vortex include the distance from the propeller centre to the free surface divided by the propeller radius and the axial velocity at the propeller plane divided by the free stream velocity. The color of the data points specifies if ventilation is observed or not. *Figure 6* include the whole range of tested propeller revolutions i.e.  $n \geq 9rps$ . According to Shiba [18] the influence of the Weber's number disappears above the so-called minimum Weber number, which is approximately 180. For our experiments a Weber number larger than 180 corresponds to a propeller speed  $n \geq 13rps$ , meaning that for the 9 and 12rps tests, surface tension related scale effects might influence the results. *Figure 7* presents the results only for tests with propeller revolutions  $n \geq 13rps$ , hence the influence of Weber's number can be neglected. In both figures, lines to divide the domain into different ventilation categories are tentatively included. These lines might be used (with care) to predict what type of ventilation that might appear in a given operational condition. Both plots are based on tests with two different model propellers; P1374:  $D=250mm$ ,  $P/D=1.1$ ,  $EAR=0.6$ ,  $z=4$ , and P1440:  $D=200mm$ ,  $P/D=1.2$ ,  $EAR=0.447$ ,  $z=4$ .

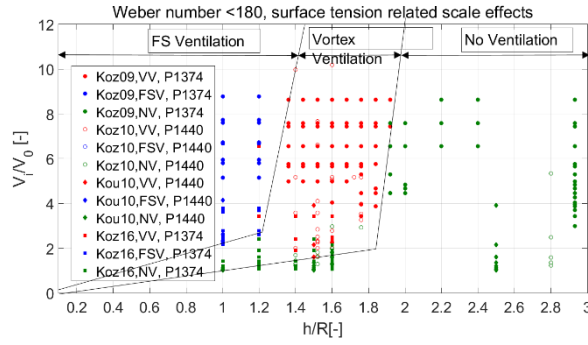


Figure 6: Experimental data showing the boundary between the vortex forming and no vortex forming flow regimes for marine propellers operating in transient condition (from low to high advance speed), propeller revolutions: ( $n \geq 9\text{Hz}$ ,  $We \geq 132$ ). Acronyms included in the legend: VV means ventilation by vortex formation, FSV means free surface ventilation, NV means no ventilation, P1374: propeller model ( $D=250\text{mm}$ ,  $P/D=1.1$ ,  $EAR=0.6$ ,  $z=4$ ), P1440: propeller model ( $D=200\text{mm}$ ,  $P/D=1.2$ ,  $EAR=0.447$ ,  $z=4$ ).

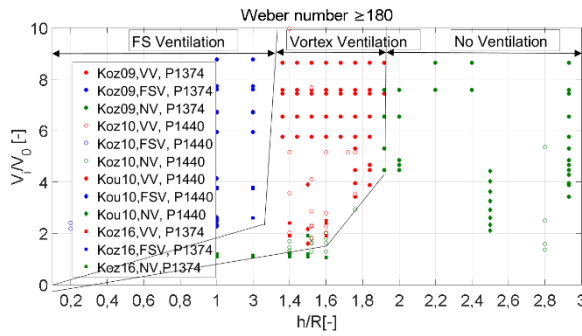


Figure 7: Experimental data showing the boundary between the vortex forming and no vortex forming flow regimes for marine propellers operating in transient condition (from low to high advance speed), propeller revolutions ( $n \geq 13\text{Hz}$ ,  $We \geq 180$ ). Acronyms included in the legend: VV means ventilation by vortex formation, FSV means free surface ventilation, NV means no ventilation. P1374: propeller model ( $D=250\text{mm}$ ,  $P/D=1.1$ ,  $EAR=0.6$ ,  $z=4$ ), P1440: propeller model ( $D=200\text{mm}$ ,  $P/D=1.2$ ,  $EAR=0.447$ ,  $z=4$ ).

#### 4. COMPARISON BETWEEN CAVITATION AND VENTILATION PHENOMENON

##### 4.1 Comparison between PHVC, and PFSVV occurrence and flow field

Sato et. al. [17] classified flow patterns for three different categories: downstream vortex, double vortex and upstream vortex flow, see Figure 8. Downstream vortex flow situation occurs when the reverse flow become stable and a vortex pattern can be detected just above the propeller. For right-handed propellers this vortex is rotating in a clockwise direction. Double vortex flow occurs for small clearance/Diameter  $c/D$  ratios ( $c/D < 0.11$ ). A counter clockwise vortex is located on the portside of the clockwise rotating vortex. Upstream vortex flows occur when the counter clockwise vortex move close and hence absorbs the clockwise vortex. As we can see from Figure 9 and Figure 10 the ventilation vortex formation is very similar to the propeller hull vortex cavitation phenomenon. We can also observe three types of the ventilating vortex impact on the propeller blades: impact on the port side, starboard side of the propeller blade as well as impact of both vortices on the blade, see Figure 10.

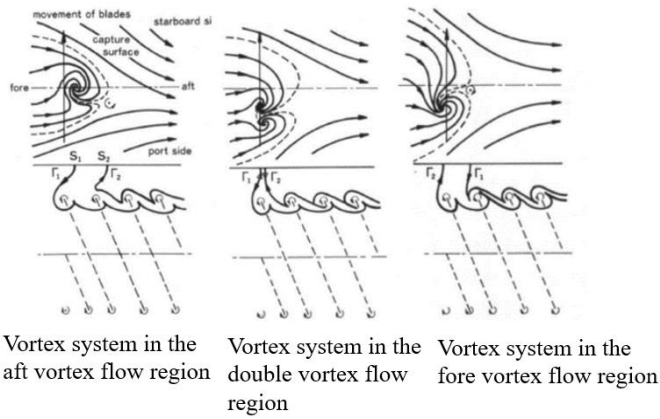


Figure 8. Vortex system (PHVC) in the aft vortex flow region (left), double vortex flow region (middle), fore vortex flow region (right), Sato et. al. [17]

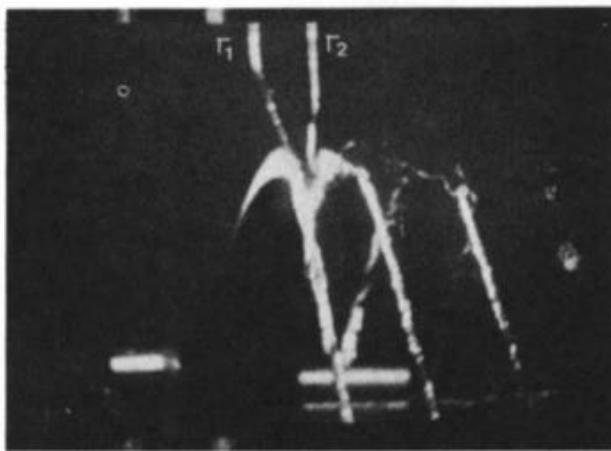
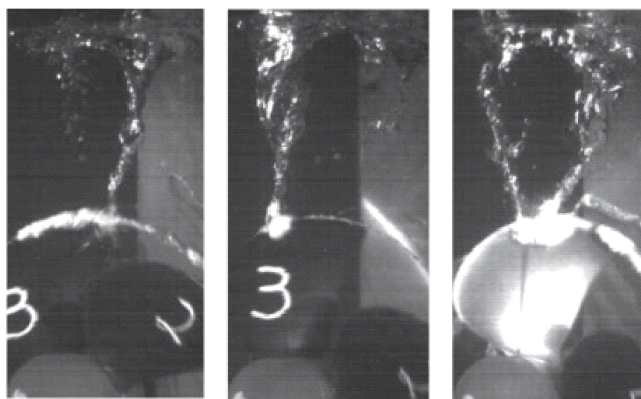


Figure 9: Two PHVC,  $c_T=11.8$ ,  $c/D=0.2$ , Nishiyama [14]



(a) Impact of the port side vortex on the blade,  $t=5.497s$ .

(b) Impact of the starboard side vortex on the blade,  $t=10.307s$ .

(c) Impact of both vortices on the blade,  $t=10.649s$ .

Figure 10: PFSVV,  $h/R=2.04$ ,  $J=0.075$  ( $c_T=253$ ,  $c/D=0.52$ ), Califano [2]

Numerical RANS simulation performed by Martio et.al. [12] shows reasonably good agreement between the vortex flow observations and calculations, see Figure 11. It was observed by Martio et.al. [12] that the oscillation amplitude of  $K_T$  reduced significantly between advance numbers 0.249 and 0.326. Still both situations produce double vortex flow condition as shown on Figure 11. The traced streamlines at  $J=0.326$  and  $J=0.433$  illustrate that for these cases the generated vortices on the free surface do not interact with a blade at any position. This is

probably explaining why the fluctuations of the thrust coefficient is strongly reduced between  $J=0.249$  and  $J=0.326$ . We observe the similar correlation for ventilation vortex phenomena. Above the so-called critical advance coefficient ( $J_C$ ) we observe that thrust loss due to ventilation is much smaller than for advance ratios below this critical advance coefficient. This is probably because that for higher advanced ratios the generated vortices on the free surface do not interact with the propeller, so the ventilation does not reach the propeller blades, see *Figure 12*. The other reason for this is that the suction (described as propeller load factor  $C_T$ ) which is generated by the propeller is smaller for higher advance ratios.

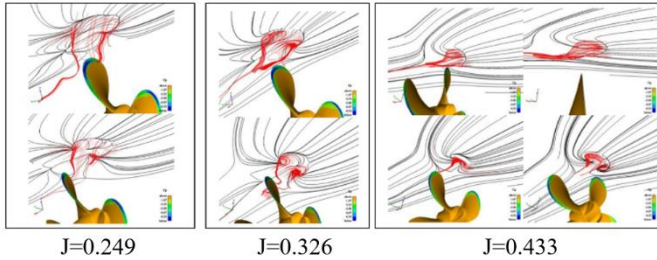


*Figure 11: The streamlines and the distribution of  $c_p$  on the suction side (PHVC),  $c/D=0.157$ ,  $n=11.8$  rps,  $D=227$ ,  $z=4$ ,  $P/D=1.1$ , Martio et. al. [12]*

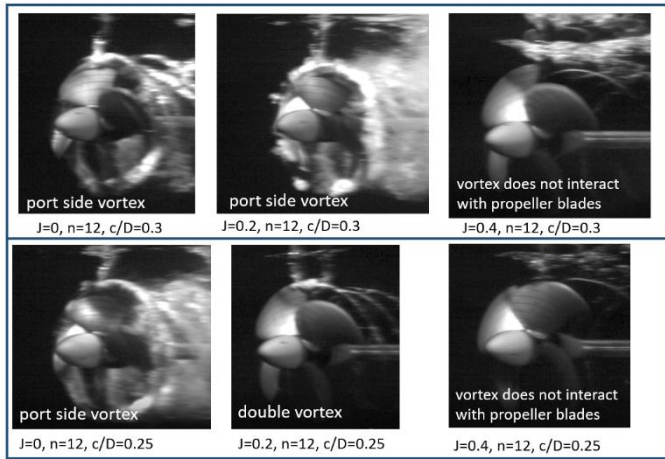


*Figure 12: Appearance of ventilation for different advance ratios,  $c/D=0.25$ ,  $0.3$  and  $n=12$  rps, (Koz16)*

#### 4.2 Ventilation regimes and critical advance ratios

The propeller might be non-ventilated, partially or fully ventilated, depending on several factors, where submergence and advance number are clearly important. Olofsson [15] divided these ventilation states into regimes illustrated in *Figure 13*. The partially ventilating regime is characterized by having varying part of the propeller blade covered by air. In this regime propeller thrust fluctuates rapidly. The regime is quite stable in time and lead to considerably reduced thrust. The propeller might also experience transition between fully and partially ventilated flow regimes. The range of advance numbers where this happens is called the unstable regime or transition regime. The sketch in *Figure 13* originally published in Olofsson [15] is based on experiments with surface-piercing propellers (meaning propellers designed to operate submerged to the propeller center). Thus, it is of interest to make a similar plot based on experiments with normal, non-ventilating propellers that are ventilating due to insufficient submergence. Such a plot has been made based on the four experimental campaigns listed in *Table 1* and is shown in *Figure 14*. The main difference between these two plots is for non-ventilated and partially ventilated flow regimes. For submergences  $h/R \geq 1.4$  we observe only two different flow regimes, Ventilation starts from the unstable regime (thus it is partially ventilated) and we do not observe the fully ventilated flow regime where the thrust loss is significant and stable.

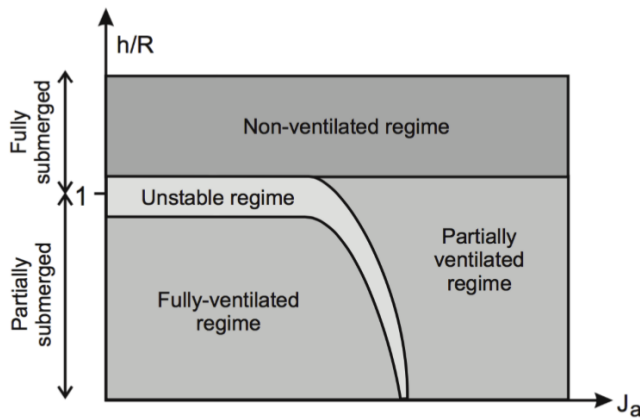


Figure 13: Ventilation flow regimes Olofsson [15], surface piercing propellers

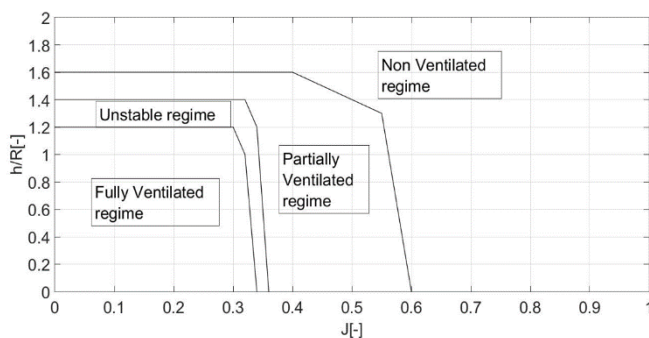


Figure 14: Ventilation flow regimes for a conventional propeller based on experiments that are listed in Table 1

Which of the three different flow regimes the propeller is operating in has a significant impact on the propeller thrust, as one can see from Figure 16 and Figure 17. The open water curve for the deeply submerged ( $K_{Tn}, K_{Qn}, \eta_{an}$ ) and ventilated ( $K_T, K_Q, \eta_a$ ) propeller is presented in Figure 15.

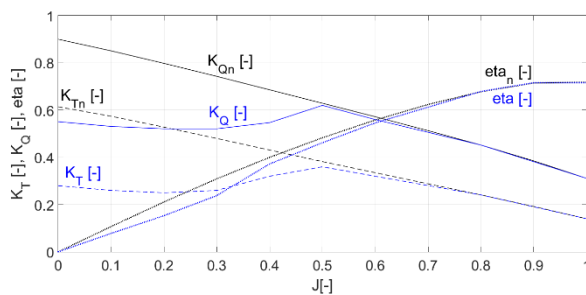


Figure 15 Open water curve for deeply submerged ( $K_{Tn}, K_{Qn}, \eta_{an}$ ) and ventilated ( $K_T, K_Q, \eta_a$ ) propeller

In the fully ventilated regime when the propeller is highly loaded and fully ventilated, thrust loss is significant and quite stable, both in time and in the sense that a further reduction of the advance number does not change the propeller thrust coefficient  $K_T = T/\rho n^2 D^4$ . The advance coefficient is below the super critical advance coefficient  $J_{SC}$ . Above the super critical advance coefficient  $J_{SC}$  and below the critical advance coefficient  $J_C$  is the unstable regime, where the propeller is partially ventilated. This regime is characterized by large variation in time of the amount of ventilation and the amount of thrust loss. Above  $J_C$  is the sub critical regime, where the propeller is non ventilated or experiencing limited ventilation. For deeper submergences ( $h/R=1.5, h/R=1.6$ ) we observe only two different ventilation regimes, ventilation starts from the unstable regime at  $J=0$  and we do not observe the super critical ventilation regime, see Figure 17. Test results are presented in the form of total thrust loss factor  $\beta_T = K_T/K_{Tn}$  where  $K_{Tn}$  is the time-averaged mean value of the thrust coefficient at the relevant advance coefficient  $J$  obtained from the calm water, deeply submerged non-ventilated propeller. Due to the torque (15Nm) and force (400N) limits of the dynamometer the range of  $J$  values for the higher revolutions speeds ( $n \geq 14Hz$ ) had to be

limited especially for larger submergences ( $h/R > 1.2$ ). This is the reason why we present super critical, unstable and sub critical ventilation regime for different propeller revolutions ( $n=16\text{Hz}$  for  $h/R=1.0, 1.2$  presented in *Figure 16* and  $n=12\text{Hz}$  for  $h/R=1.6, 1.5$  presented in *Figure 17*). As the result the surface tension scale effects might influence the results. According to Shiba [18] the influence of the Weber's number disappears above the so-called minimum Weber number, which is approximately 180. For our experiments a Weber number larger than 180 corresponds to a propeller speed  $n \geq 13\text{rps}$ , meaning that for the 9 and 12rps tests, surface tension related scale effects might influence the results.

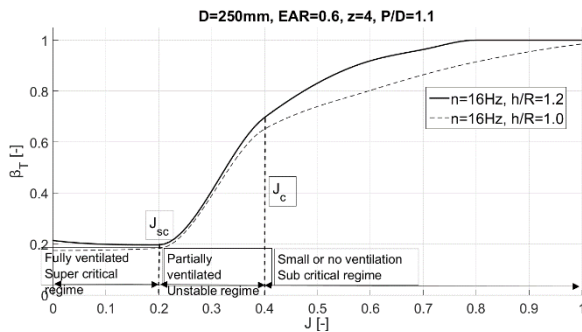


Figure 16: Super critical, unstable and sub critical ventilation regime presented for  $h/R=1.0$  and  $1.2$ , (Koz16)

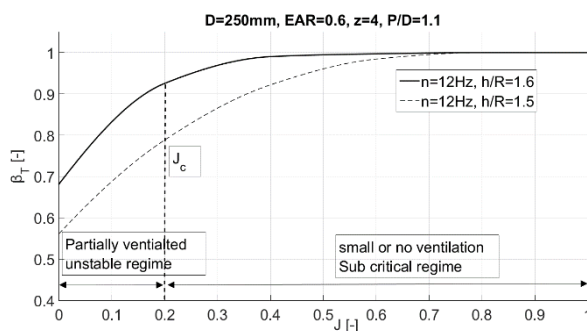


Figure 17: Unstable and sub critical ventilation regime presented for  $h/R=1.6$  and  $1.5$ , (Koz16)

### 4.3 Inception of cavitating /ventilating vortex

Inception of vortex cavitation is a complicated issue because it involves a vortex with a low pressure region in the core, but also nuclei to expand in that vortex core. When a cavitation nuclei reach a critically low pressure it will rapidly expand so that the cavitation is formed.

Cavitation inception depends on the minimum pressure in the vortex core. The velocity distribution of a 2D vortex flow as given by two different vortex models is shown in the *Figure 18* below.

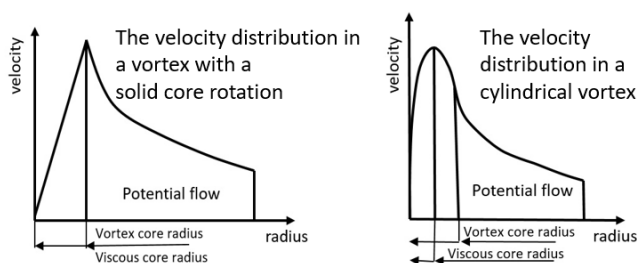


Figure 18: The velocity distribution on the vortex flow

The pressure distribution in the center of a vortex is lower than in the surrounding fluid because of the centrifugal effects of the rotating fluid. In a cylindrical vortex this can be easily derived from the force equilibrium on a fluid

particle in rotating flow. A rotating particle which follows a cylindrical path around the vortex core is subjected to a centrifugal force, which has to be compensated by a pressure force in the radial direction

$$\frac{\partial p}{\partial r} = \rho \frac{v(r)^2}{r} \quad (1)$$

In the case of a Rankine vortex, the pressure integration over radius  $r$  from  $a$  to  $\infty$  results in

$$p_\infty - p(a) = \frac{\rho \Gamma^2}{4\pi^2 a_v^2} \quad (2)$$

Where  $a_v$  is the radius of the cavitating/ventilating vortex and  $\Gamma$  is the circulation strength.

For a ventilating vortex, the pressure in the center of the vortex is typically assumed to be equal to the atmospheric pressure,  $p_{at}$  while the pressure far away from the vortex,  $p_\infty = p_{at} + \rho gh$  so we can express equation (2) as:

$$p_{at} + \rho gh - p_{at} = \frac{\rho \Gamma^2}{4\pi^2 a_v^2} \quad (3)$$

The problem now is to estimate the radius of the viscous core at which ventilation inception starts. To this end, we first need to find the strength of the circulation  $\Gamma$ . This is difficult, and a simplified approach is taken. The circulation should increase with the propeller loading, and it seems reasonable to link it to the circulation of a propeller blade. Therefore, we start with using the known approximate relation between propeller blade lift coefficient at 70% radius  $c_{L0.7}$ , thrust coefficient for non-ventilated, deeply submerged propeller  $K_{Tn}$  and blade area ratio  $EAR$ , which is valid as an approximation for typical conventional propellers Gutsche [4]:

$$c_{L0.7} = \frac{K_{Tn}}{1.5EAR} \quad (4)$$

Using the Kutta Joukowski theorem, the lift coefficient can be linked to the circulation at the same blade section:

$$c_{L0.7} = \frac{\rho \Gamma V_c}{0.5 \rho V_c^2 c_{0.7}} \quad (5)$$

Where  $V_c$  is the local relative velocity at the blade section, which, when ignoring induced velocities can be calculated as  $V_c = \sqrt{V_A^2 + (0.7\pi nD)^2}$  where  $n$  is the propeller speed. By combining the two expressions for the lift coefficient, the expression for the circulation strength is obtained:

$$\Gamma = \frac{V_c c_{0.7} K_{Tn}}{3 \cdot EAR} \quad (6)$$

By using the equation (6) to express the circulation we obtain a formula for the radius of ventilating vortex

$$a_v = \frac{(V_c c_{0.7} K_{Tn}) / (3 \cdot EAR)}{2\pi \sqrt{gh}} \quad (7)$$

A question that remains is how large the radius  $a_v$  needs to be for ventilation to occur. For very small radii, the air flow velocity increases, leading to decreasing air pressure, so that the assumptions about atmospheric pressure used for deriving equation (3) is no longer valid. Decreasing air pressure means reduced radius, so assuming atmospheric pressure means that we over-predict the vortex core radius, especially for small radii. To correct for this effect, we need to know the air flow rate, something which is really quite hard to calculate, since it involves how the air is swept from the propeller into the free stream.

From the experiments, presented in *Table 1*, it is found that ventilation does not occur for bollard condition  $J=0$  for propeller submergences over 3.4, see Kozłowska et. al. [9]. Based on this observation we calculated, according to equation (7), that the minimum vortex core for ventilation to occur is equal to 3.3 mm for  $n=16\text{Hz}$ . *Figure 19* presents the calculation for the radius of ventilating vortex for different submergences ( $h/R=2.0, 1.8, 1.6, 1.4, 1.2$ ) and advance ratio from 0 to 0.7, based on equation (7). If we assumed that the minimum vortex radius for the propeller to ventilate is 3.3 mm we can then calculate the maximum advance ratio for different submergences for a propeller to ventilate, see *Table 4*. When we know the advance ratio and the propeller characteristics, it is straight

forward to calculate also other parameters like the velocity through the propeller  $V_i$ , and the two formulations for propeller thrust coefficient  $c_{Tn}$  and  $K_{Tn}$ . If one wants to use the data in Table 4 to estimate when vortex ventilation might occur for other propellers than the ones studied here, it is recommended to use a pitch-independent parameter like  $V_i$ . The minimum vortex radius will probably depend on the amount of air sucked through it, since a stronger air flow will reduce the pressure below atmospheric (which is the current approximation). Thus, the stronger the ventilation air flow, the larger the calculated minimum radius needs to be. An implication of this is that the calculated minimum radius will need to be bigger for full scale. How much is hard to say without quantifying the amount of air sucked through the vortex.

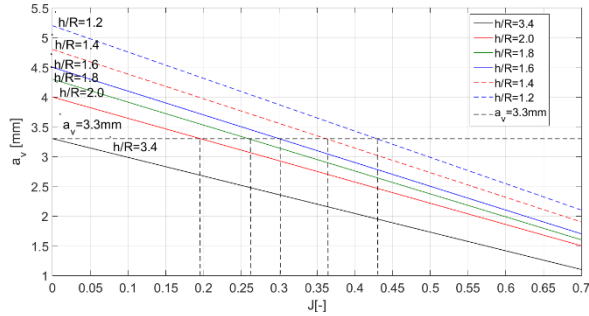


Figure 19: Minimum vortex radius for ventilation to occur for  $n=16\text{Hz}$

$a_v$ [mm]	$h/R$ [-]	$J_{max}$ [-]	$V_i$ [m/s]	$V_i/V_0$ [-]	$c_{Tn}$ [-]	$K_{Tn}$ [-]
3.3	3.4	0.000	2.51	-	-	0.62
3.3	2.0	0.195	2.74	3.52	35.39	0.53
3.3	1.8	0.260	2.83	2.72	18.77	0.50
3.3	1.6	0.300	2.89	2.41	13.57	0.48
3.3	1.4	0.360	2.98	2.07	8.87	0.45
3.3	1.2	0.440	3.11	1.77	5.44	0.41

Table 4: Maximum advance ratio ( $J_{max}$ ) for ventilation to occur based on minimum radius of the vortex core  $a_v$

Comparison between the calculation of the maximum advance ratio for ventilation to occur for different submergence ratios presented in Table 4 based on the minimum radius of the vortex core correspond quite well with experiments, see Figure 20 and Figure 21. For deeply submerged propeller  $h/R=2.04$  we observe ventilation for  $J=0.1$  and  $J=0.133$ , which correspond with the maximum advance ratio  $J_{max} = 0.195$ . For  $h/R=1.6$  we observe that ventilation stops above the  $J=0.2$ , which correspond with the maximum advance ratio  $J_{max} = 0.3$ . For propeller submergence  $h/R=1.2$  we observe very little amount of ventilation for  $J>0.4$ .

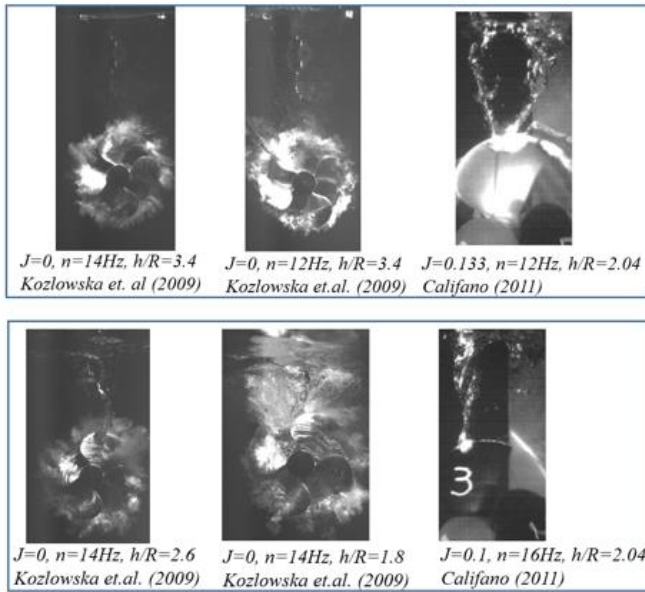


Figure 20: Ventilation inception by vortex formation based on experiments presented in Table 1

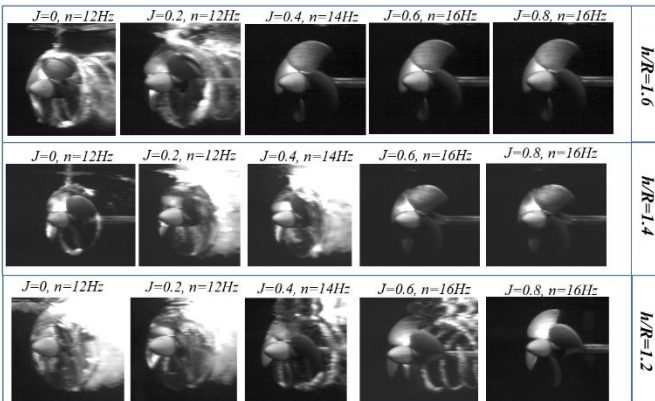


Figure 21: Ventilation inception by vortex formation based on experiments presented in Table 1

If is of interest to compare the outcome of equation (7), given in Table 4, with the boundary lines in Figure 7. Such a comparison is given in Figure 22. It can be seen that the agreement between the two methods is good, given the inherent uncertainties in the observations that these methods are based on. The agreement is particularly good for  $h/R < 1.8$ . For deeply submerged propellers the alternative method seems to over-predict the maximum advance ratio for ventilation, which might be caused by neglecting the effect of the air flow on the vortex core radius, as previously mentioned.

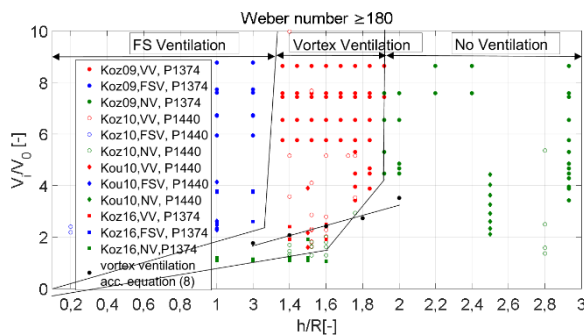


Figure 22: Comparison between alternative method of calculating if vortex ventilation will happen according to equation (7), and the boundary between vortex forming and non-vortex forming flow regimes, presented in Figure 7.

## 5. CONCLUSIONS

An analysis of the experimental data allows to define the boundaries between appearance or absence of ventilation by vortex formation for marine propellers working near the free surface. The factors determining the formation of vortex include propeller radius divided by the distance from the propeller to the free surface and the axial velocity at the propeller plane divided by the free stream velocity.

It has been shown that the vortex forming mechanism of Propeller Hull Vortex Cavitation (PHVC) is closely related to the mechanism of Propeller Free Surface Vortex Ventilation (PFSV) ventilation. The vorticity is formed by strong hydrodynamic interaction between the propeller and hull (or plate) (PHVC) and between propeller and free surface (PFSVV), which is further developed into a vortex. The occurrence of the PHVC and PFSVV depends on the propeller load coefficient  $c_T$ , tip clearance ratio  $c/D$  and flow cavitation or ventilation number.

It has been described by Martio et. al. [12] that the oscillation amplitude due to PHVC reduced significantly between advance numbers 0.249 and 0.326 even if still both situations produce the double vortex flow conditions. The numerical investigation shows that for these cases the generated vortices for high advance ratios ( $J=0.325$  and  $J=0.433$ ) do not interact with propeller blades at any blade positions. We observe the similar correlation for ventilation vortex phenomena. Above the so-called critical advance coefficient, we observe that thrust loss due to ventilation is much smaller than for advance ratios below critical advance coefficient. This can probably be explained by the observation that for higher advance ratios the generated vortices do not interact with the propeller thus the ventilation does not appear on the propeller blades. The relation between the cavitating/ventilating vortex and the pressure in the core of a given vortex was investigated in order to define the vortex ventilation inception. As the result we obtain a formula for the radius of cavitating/ventilating vortex which depends on the propeller circulation and the cavitation/ventilation number. Therefore, the relation between the ventilating minimum vortex core radius and the maximum advance ratio for ventilation to occur can be used to define ventilation inception.

## 6. ACKNOWLEDGEMENT

This work has been carried out at the University Technology Centre of Rolls Royce at NTNU (Trondheim) sponsored by Rolls Royce Marine. We would like to thank the technicians and staff at MARINTEK for their help and expertise in performing the experiments.

## REFERENCES

- [1] Bissinger, N. C. and Braun, G. W. (1974) "On the inlet vortex system", *NASA CR-132536*
- [2] Califano, A. (2011) "Dynamics loads on marine propellers due to intermittent ventilation", *PhD thesis, Norwegian University of Science and Technology*, Trondheim
- [3] Denny D. (1956) "Experimental study of air entering vortices in pump sumps". *Institution of Mechanical Engineers- Proceedings*, 170(2):106-116
- [4] Gutsche, F. (1962) "Der Einfluss der Kavitation auf die Profileigenschaften von Propellerblattschnitten", *Schiffbau Forschung*, Heft 1, 196
- [5] Huse, (1971) "Propeller- Hull Vortex Cavitation". *Norwegian Ship Model Exp. Tank Publ.*, May 1971
- [6] Hutchinson, S., Steen, S. (2013) "Modelling of propeller hydrodynamics for implementation with multibody simulation". *Dresdner Maschinenelemente Kolloquium:3. und 4.Dezember 2013*. Dresden: TUDpress Verlag der Wissenschaften Dresden 2013 ISBN 978-3-944331-33-1, s. 365-384, MARINTEK NTNU
- [7] Jermy, M. and Ho, W. (2008) "Location of the vortex formation threshold at suction inlets near ground planes by computational fluid dynamic simulation". *Proceedings of the Institution of Mechanical Engineers, Part G: Journal of Aerospace Engineering*
- [8] Koushan, K., Silas Spence, Luca Savio; (2011) "Ventilated Propeller Blade Loadings and Spindle Moment of a Thruster in Calm Water and Waves" *Proceedings of Second International Symposium on Marine Propulsors*, smp11, Hamburg, Germany.
- [9] Kozłowska A. M. , Steen S., Koushan K. (2009) 'Classification of Different Type of Propeller Ventilation and Ventilation Inception Mechanisms' *SMP 09, Trondheim, Norway*.
- [10] Kozłowska, A. and Steen, S. (2010) "Ducted and open propeller subjected to intermittent ventilation", *Eighteen International Conference on Hydrodynamics in Ship Design, Safety and Operation*, Gdansk, Poland
- [11] Kozłowska, A. Wockner, K., Rung, T., Steen, S. (2011) "Numerical and Experimental study of propeller ventilation" *Proceedings of Second International Symposium on Marine Propulsors*, Hamburg, Germany

- [12] Martio, J. Sipila, T., Sanchez-Caja, A., Saitso, I., Siikonen, T., (2011) "Evaluation of propeller hull vortex cavitation using a RANS solver". Proceedings of Second International Symposium on Marine Propulsors, Hamburg, Germany
- [13] Nakayama, A and Jones, J.R. (1996) "Vortex formation in inlet flow near the wall". In 34<sup>th</sup> Aerospace Science Meeting and Exhibit, AIAA 96-0803
- [14] Nishiyama, S. (1986) "Experimental Research on propeller-hull vortex cavitation". In Transactions of the West Japan Society of Naval Architects.
- [15] Olofsson, N. (1996) "Forces and Flow Characteristics of Partially Submerged Propeller", PhD thesis, Chalmers Tekniska Hogskola.
- [16] Rodert, L.A., Garret, F. B. (1955) "Ingestion of foreign objects into turbine engines by vortices", NACA TN 3330
- [17] Sato, et. al. (1986) "Observation of Flow on a Horizontal Flat Plate above a Working Propeller and Physisc of Propeller- Hull Vortex Cavitation" Proceed. Internat.Symposium on Propeller and Cavitation, Wuxi, China
- [18] Shiba H. (1953) Air-drawing of marine propellers. Technical report 9, Transportation Technical Research Institute